*Materials Research*. 2025; 28: e20250317
DOI: https://doi.org/10.1590/1980-5373-MR-2025-0317

# Porous $Si_3N_4$ Ceramics Prepared by Gelcasting Route and Pressureless Sintering at Different Temperatures

***Regina O. da Silva*[a], *Rubens Chiba*[a], *Thiago S. Ferreira*[a], *João V.B. Reis*[a],**

***Flávio M.S. Carvalho*[b], *Daniel P. Vieira*[a], *Cecilia C. Guedes-Silva*[a]***

[a]*Instituto de Pesquisas Energéticas e Nucleares, Comissão Nacional de Energia Nuclear, Av. Prof. Lineu Prestes, 2242, 05508-000, São Paulo, SP, Brasil.*
[b]*Universidade de São Paulo, Instituto de Geociências, Rua do Lago, 562, 05508-080, São Paulo, SP, Brasil.*

Received: February 13, 2025; Revised: July 05, 2025; Accepted: July 13, 2025

In this work, the gelcasting method was used to prepare porous $Si_3N_4$ ceramics, using sodium lauryl sulfate and Isobam 110 as foaming and gelling agents, respectively. Samples sintered at different temperatures were characterized by mercury porosimetry, X-ray diffraction, scanning electron microscopy, and compressive strength. The findings demonstrated that the samples had a porosity ranging from 53.6 to 67.21%, featuring a porous structure with interconnected pores with average pore size varying between 89.20 and 158 μm and pore throats of ~0.3-0.5 μm. α-$Si_3N_4$, β-$Si_3N_4$, $CaSiO_3$, and $Ca_3SiO_5$ phases were identified in all porous ceramics. Increased β-$Si_3N_4$ content, density, and compressive strength were observed in ceramics sintered at higher temperatures. Even when the samples reached a porosity of 67.21%, the compressive strength remained relatively high, with a value of 59.36 MPa. As a result, the porosity and strength of the porous $Si_3N_4$ ceramics were well-balanced due to the efficient use of gelcasting method

**Keywords:** *gelcasting, silicon nitride, porosity, sintering.*

## 1. Introduction

Due to their characteristics, such as high specific surface area, high stability, and low thermal conductivity, porous ceramics have attracted the attention of researchers for use as catalyst supports, bioceramics, chemical fillers, heat insulators, and filtration materials. However, obtaining ceramic materials with controlled pore size and distribution remains a technological challenge[1,2]. In recent years, porous silicon nitride ($Si_3N_4$) ceramics have gained attention due to their high biocompatibility, low thermal expansion, high mechanical properties, and controlled permeability[3]. Different methods can be used to prepare porous silicon nitride, including partial sintering[4], direct foaming[5], freeze-drying[6], sacrificial, and gelcasting[7].

Gelcasting is an attractive technique because of its ability to produce complex parts, strength green compacts with low organic content, and a final material with homogeneous properties[8]. For instance, Zou et al.[9] prepared porous silicon nitride ceramics using gelcasting route followed by gas pressure sintering (GPS). Acrylamide (AM) and N,N'-methylenebisacrylamide (MBAM) were employed to obtain slurries with solid loading of 46.5 vol. %. They found that the bending strength (205.2 – 218.4 MPa) and elastic modulus (63.1 – 80.4 GPa) were influenced by the samples' porosity which varied from 27.5 to 33.6%. Chen et al.[10] also produced silicon nitride with a homogeneous pore structure by gelcasting using AM and MBAM as monomer and crosslinker, respectively. The ceramics reached high porosity (67.83 to 78.03%) and compressive strength of 11.79 to 47.55 MPa owing to the low solid contents (10 to 25 vol. %) and the development of a microstructure with interlocked elongated grains.

Although acrylamide (AM) and methylenebisacrylamide (MBAM) are used as monomer in aqueous gelcasting, other systems with lower toxicity have been developed. Silicon nitride foams with high porosity (76.3-83.8%) and a hierarchical structure were produced by Li et al.[11] using aqueous gelcasting and egg as the gelling and foaming agent. The samples presented a compressive strength of 18 MPa and gas permeability of 5.16 $(cm^3.cm)/(cm^2.s.kPa)$, essential characteristics for industrial dust filtration. Moraes et al.[12] studied different gelling agents (egg albumen, agar-agar, and methylcellulose) to prepare silicon nitride foams with 30 vol.% of solids by gelcasting method. Bubbles were introduced into the slurries through surfactant additions (Tergitol TNM-10) and stirring, resulting in samples with porosities of up to 89% and compressive strengths of up to 33.5 MPa.

In 2013, Yang et al.[13] introduced a nontoxic copolymer with functional groups such as –COO–, –$CONH_2$, and –CO–O–CO–, commercially called Isobam, as a gelling agent in gelcasting method of ceramics. Small amounts of Isobam (<1 wt.% of powder) can spontaneously complete the gelation

*e-mail: cecilia.guedes@ipen.br
**Associate Editor**: Celso Santilli.
**Editor-in-Chief**: Luiz Antonio Pessan.

process at room temperature, generating homogeneous green bodies[14]. Wan et al.[15-17] prepared porous silicon nitride by Isobam gelcasting method indicating essential results. Firstly, $Si_3N_4$ samples were pressureless sintered from 25 – 40 vol.% suspensions ($Si_3N_4$ and $Y_2O_3$ powders) and 0.2 wt.% Isobam[15]. The process demonstrated good performance, producing ceramics with flexural strengths of 119–167 MPa and porosities of up to 56%. Later, they obtained silicon nitride foams by introducing corn starch as a pore-forming agent into slurries containing $Si_3N_4$, BN, and various rare earth oxides[16]. In that work, it was possible to produce porous ceramics with higher porosity and better mechanical properties, depending on the rare oxide used as a sintering aid. Wan et al.[17] also found that the Isobam concentration influences both the slurry viscosity and pore structure in porous silicon nitride ceramics with unidirectionally oriented pores, resulting from solidification, nitridation, and post-sintering.

This work aimed to fabricate, for the first time, silicon nitride porous ceramics using foam-gelcasting, with Isobam 110 as the gelling agent and sodium lauryl sulfate as the foaming agent. This novel combination enables the production of green bodies through room-temperature gelation and porous sintered ceramics, eliminating the need for a sacrificial phase. The approach offers significant advantages in terms of cost-effectiveness and sustainability, marking a unique advancement in the field. Additionally, the effect of varying sintering temperatures on the microstructure and mechanical properties was also evaluated.

## 2. Experimental Procedure

### *2.1. Raw materials*

The starting materials used were α-$Si_3N_4$ powders (UBE, SN-E10, 95 wt.% α-$Si_3N_4$), $SiO_2$ (quartz, 99.9% purity, Sigma-Aldrich), and $CaCO_3$ (P.A., Vetec). Isobam 110 (molecular weight 160,000–170,000, Kuraray Co. Ltd) and sodium lauryl sulfate (SLS) were used as gelling and foaming agents in the gelcasting process, respectively.

### *2.2. Samples preparation*

Initially, the raw materials were mixed after dosing to prepare a ceramic composition with 90 wt.% $Si_3N_4$, 5 wt.% $SiO_2$ and 5 wt.% CaO, coded as 90$Si_3N_4$-5$SiO_2$-5CaO. $SiO_2$ and CaO were used as sintering aids. This additive formulation was selected based on the low-temperature eutectic liquid phase formed due to the reaction with the $SiO_2$ coating already present on $Si_3N_4$[18] and its efficiency in sintering silicon nitride ceramics[19]. The composition was ball milled for 24 h using alumina balls in isopropanol and then dried in a rotary evaporator at 90 °C. Slurries containing 28 vol.% 90$Si_3N_4$-5$SiO_2$-5CaO powder and deionized water with a pH around 12, previously adjusted with $NH_4OH$, were ball milled with $Al_2O_3$ balls for 24 h. The slurries were rheologically characterized at room temperature using a First Plus model viscometer (Lamy Rheology Instruments) under shear rates ranging from 10 to 100 $s^{-1}$.

After adjusting the pH at 10.23 to 12.00 through variations in $NH_4OH$ addition, 1.0 wt.% SLS and 0.5 wt. % Isobam were added to the slurries under vigorous stirring for 3 min. The foamed slurry was poured into silicone molds for gelation at room temperature. After 24 hours, the green bodies were removed from the molds and sintered in a nitrogen atmosphere at a heating rate of 10°C/min, reaching temperatures of 1550, 1600, 1650, and 1700°C for 1 hour each.

### *2.3. Characterization*

Morphological and microstructural characterizations were performed by scanning electron microscopy (SEM, Hitachi TM-3000) of the fractured surface of ceramics coated with gold. The pore size distribution was determined using a mercury intrusion porosimeter (AutoPore IV Micromeritics), which measures pore diameters from 0.003 to 360 µm. ImageJ software was also used to measure pore size[20]. For the analyses, a single representative specimen from each type of porous ceramic was selected. The apparent porosity (Equation 1) and apparent density (Equation 2) of the sintered samples were determined using 15 specimens of each porous ceramic. Measurements were obtained through the liquid immersion method based on Archimedes' principle, with distilled water as the immersion medium.

$$Apparent\ density\left(g/cm^3\right)=\frac{m_1}{m_3-m_2}x\rho \quad (1)$$

$$Apparent\ porosity\left(\%\right)=\frac{m_3-m_1}{m_3-m_2} \quad (2)$$

Where $m_1$ = dry weight (g), $m_2$ = suspended weight (g), $m_3$ = soaked weight (g), and ρ = density of water (g/$cm^3$).

An X-ray diffractometer (D8 Advance Bruker, Cu Kα radiation source) operated at 40 kV and 40µÅ with step of 0.02° (2θ) and 5s/pass was used to examine the phase composition and the ratio of β- to (α+β)-$Si_3N_4$ in one individual specimen representative of ceramics sintered at different temperatures. The weight fractions of α and β-$Si_3N_4$ were estimated by Rietveld refinement using Profex software version 4.8[21]. Compressive strength was tested using a universal testing machine (Instron 4400R) with a 0.5 mm/min crosshead speed at a load cell of 5 kN. Ten specimens of each type of porous ceramic were subjected to compressive tests.

## 3. Results and Discussion

Figure 1 shows the viscosity as a function of pH for slurries at a pH ranging from 10.23 to 12.00. From this figure, it is evident that the slurries exhibit similar rheological behaviors. At a shear rate of 100 $s^{-1}$, the apparent viscosity is less than 1000 mPa.s, which satisfies the rheological property requirements for gelcasting processing[8]. Furthermore, the viscosity of the $Si_3N_4$ ceramic slurries decreases with increasing shear rate, which is an indication of a shear-thinning behavior typical of pseudoplastic fluids. In ceramics, pseudoplasticity is related to the gradual breakdown of the particles' agglomerates when shear stress is applied. At higher shear stresses, the particles tend to align in the direction of the flow, contributing to a decrease in the viscosity of the slurry. A shear-thinning behavior is necessary to form ceramics using gelcasting, as the slurries can flow under

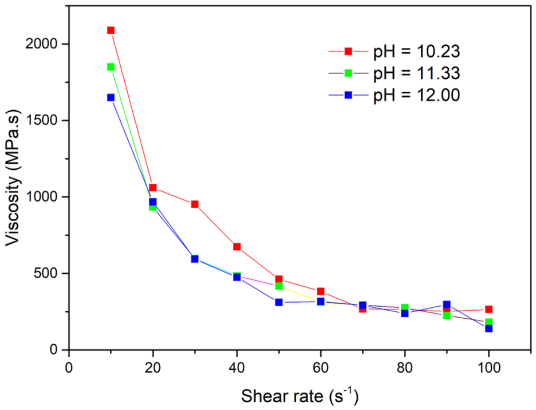


**Figure 1.** Viscosity versus shear rate at different pH values for silicon nitride slurries.

high tension during the stirring step and retain their shape after the stirring stops[22]. Pseudoplasticity is also important in preventing the collapse of bubbles that form pores in ceramic foams, as observed in this work.

Figure 2 illustrates SEM micrographs of the fractured surfaces of as-prepared samples sintered at different temperatures, along with the corresponding equivalent pore diameter distribution determined using ImageJ software[20]. The low-magnification images reveal that the fired samples have a high amount of nearly spherical pores. The equivalent pore diameters were statistically analyzed with average values of 151.98, 158.0, 128.3, and 89.20 µm for samples sintered at 1550, 1600, 1650, and 1700°C, respectively. Smaller pores into some larger pores can also be identified, creating a hierarchical porous structure with interconnected pores. While larger pores are formed by mechanical foaming during the gelcasting route, smaller ones are due to bubble coalescence during the different steps of the process, i.e., gelation, drying, and sintering[23].

Figure 3 presents the pore size distribution of all materials determined by mercury porosimetry. Compared to the porous structure observed in the SEM images, the pore sizes determined are significantly smaller, in the range of approximately 0.3 to 0.5 µm. This result can be attributed to the "bottle-neck" effect, where mercury accesses larger pores through narrow passages[24]. Hence, the pore diameters measured by mercury porosimetry correspond to the diameters of these narrow passages, known as pore throats, a crucial characteristic for applications such as filtration, catalysis, or any application requiring the movement of fluids through the ceramic. The pore throat size distributions of the ceramics show a monomodal pattern. However, as the sintering temperature increases, the curves shift to the left, indicating that smaller pore throats are predominant at higher sintering temperatures as a consequence of the densification process.

Figure 4 shows the bulk density and apparent porosity of the porous silicon nitride ceramics as a function of the sintering temperature. The apparent porosity values are closely aligned with the open porosity measurements obtained through mercury porosimetry. The apparent porosity values are 67.21, 60.73, 57.43, and 53.60%, while the corresponding open porosity values are 68.79, 62.55, 60.04, and 49.94% at sintering temperatures of 1550, 1600, 1650, and 1700 °C, respectively. Although some data scatter is present, likely due to the small specimen size (~Ø12 mm × 3 mm), the increasing trend in density and decreasing porosity with rising temperature demonstrate the influence of sintering temperature on densification. This behavior reflects established expectations in ceramic processing. Silicon nitride ceramics are covalent compounds characterized by high bond energy and low atomic self-diffusion coefficients, which make conventional sintering difficult. As a result, $Si_3N_4$ is typically densified through liquid-phase sintering (LPS), aided by oxide additives that react with the native silica layer on α-$Si_3N_4$ particles at elevated temperatures[25]. In this study, the presence of CaO (5 wt.%) and $SiO_2$ (5 wt.% as an additive plus 3.6 wt.% from the native silica layer on α-$Si_3N_4$) in the composition forms an eutectic liquid at approximately 1436 °C[18]. This eutectic point is significantly lower compared to that of conventional $Y_2O_3$–$Al_2O_3$ additives (1700 °C)[26], forming a substantial liquid phase at comparatively lower temperatures. This liquid wets the $Si_3N_4$ grains and promotes densification once the eutectic temperature is reached or exceeded. Kingery's theory[27] suggests that the LPS of $Si_3N_4$ ceramics occurs in three stages: particle rearrangement, solution–reprecipitation, and grain growth phase characterized by Ostwald ripening. The initial stage, particle rearrangement, plays a key role in the rapid shrinkage during sintering. As temperature increases, α-$Si_3N_4$ gradually dissolves into the liquid phase and reprecipitates onto β-$Si_3N_4$ nuclei, driving grain growth and promoting microstructural evolution, completing the α/β-$Si_3N_4$ transformation and densification process at approximately 1800 °C. Upon cooling, the high-temperature liquid phase transforms into a glassy or partially crystalline phase, which is usually dispersed at grain boundaries and intersections of three grains of $Si_3N_4$[28,29].

Our result is supported by a previous work[19], in which silicon nitride ceramics containing a similar additives formulation and pressureless sintered at 1815 °C, achieved a relative density of 97% along with a microstructure composed exclusively of β-$Si_3N_4$ and a secondary amorphous phase resulting from the solidification of the liquid phase formed during sintering. This demonstrates that when using 5 wt.% $SiO_2$ and 5 wt.% CaO as sintering aids, liquid-phase sintering of silicon nitride can be effectively completed at temperatures above 1800 °C. However, even when the sintering was carried out at the highest temperature (1700°C) in the present work, the ceramic reached a very low density (1.43 g/cm$^3$) and high porosity (53.60%), demonstrating that the porous structure formed during the gelcasting step was well-kept. Although higher porosity can lead to reduced mechanical properties, factors such as pore size distribution and connectivity also play a crucial role in determining characteristics like strength and hardness. Introducing porosity into the material makes it appreciated for various industries and applications, such as filters, catalyst supports, scaffolds for tissue engineering, heat exchangers, sensors, and radomes[30]. Hence, the relationship between sintering temperature, density, and porosity is crucial for optimizing the properties of porous ceramics for specific applications.

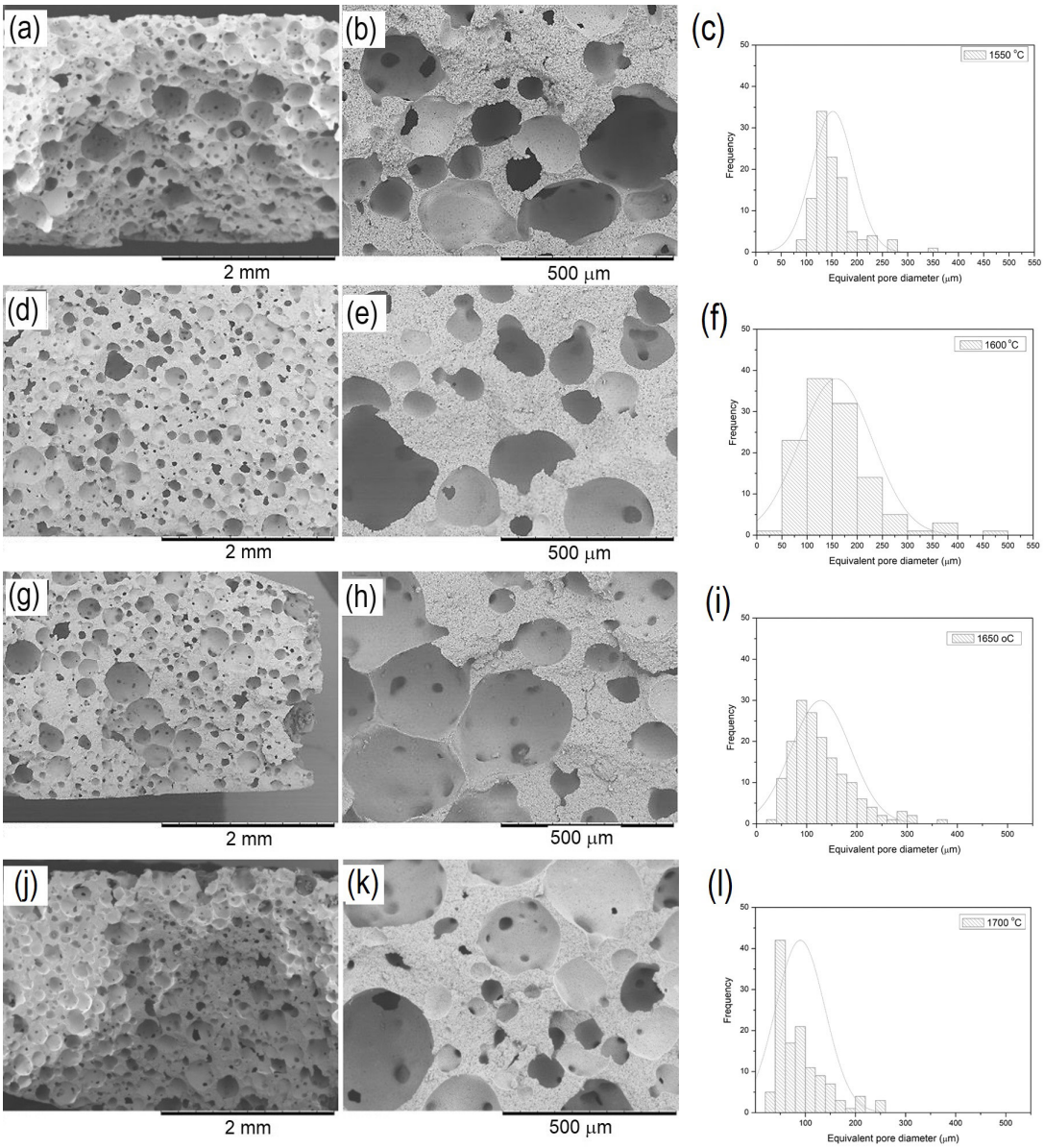


**Figure 2.** SEM images of fractured samples sintered at different temperatures for 1 hour and their equivalent pore distribution determined by Image J: (a,b,c) 1550 °C; (d,e,f) 1600 °C; (g,h,i) 1650 °C; (j,k,l) 1700 °C.

SEM images at high magnification of the porous ceramics cell walls reveal significant microstructural changes as the sintering temperature increases. Figure 5 shows that the sample sintered at 1550°C for 1 h exhibits cell walls with a morphology characterized by small equiaxed grains, typical of the α-$Si_3N_4$ phase, and micron-sized pores resulting from partial sintering. Although such equiaxed grains are also present in the sample sintered at 1600 °C for 1 h (Figure 5b), the typical long columnar grains with an interlocking arrangement can also be noticed because of the anisotropic growth of β-$Si_3N_4$ grains along the [001] and [210] directions[31]. However, increasing the temperature to 1650 and 1700 °C (Figures 5c and 5d), a more significant decrease of equiaxed grains and an increase of β-$Si_3N_4$ grains are observed. This behavior is consistent with the α/β-$Si_3N_4$ transformation mechanism. At high temperatures, β-$Si_3N_4$ is thermodynamically more stable than α-$Si_3N_4$. In addition, the ability of the formed liquid phase to flow and wet the grains is enhanced due to its reduced viscosity and increased volume, accelerating the particle rearrangement and dissolution-reprecipitation processes[29,32].

Figure 6 displays the XRD patterns of the samples sintered at 1550, 1600, 1650, and 1700 °C for 1 h, respectively. It can be found that α-$Si_3N_4$ (PDF 01-084-8319), β-$Si_3N_4$ (PDF 01-082-0697), $CaSiO_3$ (wollastonite, PDF 01-076-0925), and traces of $Ca_3SiO_5$ (PDF 00-049-0442) are present in all samples. The secondary phases $CaSiO_3$ and $Ca_3SiO_5$ are due to the crystallization of the liquid phase during the cooling

step of the sintering process. At heating, the reactions between the sintering aids[18] are:

$$SiO_2 + CaO \rightarrow CaSiO_3 \quad (3)$$

$$SiO_2 + 2CaO \rightarrow Ca_2SiO_4 \quad (4)$$

$$CaO + Ca_2SiO_4 \rightarrow Ca_3SiO_5 \quad (5)$$

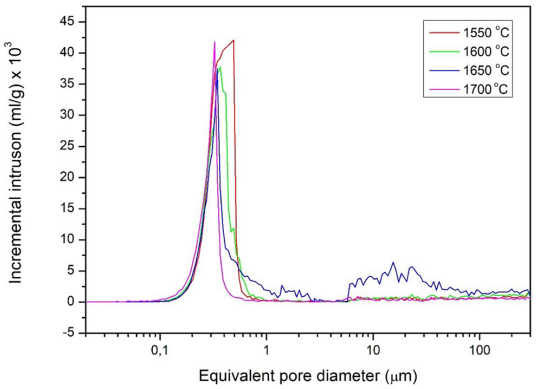


**Figure 3.** Pore size distribution of the porous silicon nitride ceramics sintered at different temperatures.

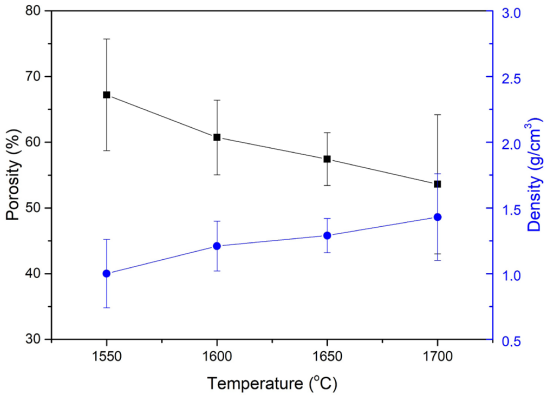


**Figure 4.** Porosity and apparent density of the studied samples obtained at different sintering temperatures.

Additionally, as shown in Figure 6, the intensity of the α-$Si_3N_4$ diffraction peaks decreases with increasing temperature. This behavior is in good agreement with the ratio of β-to (α+β)-$Si_3N_4$ (Figure 7), as calculated by Rietveld refinement and confirmed by the microstructural analysis illustrated in Figure 5. The β-$Si_3N_4$ content increases gradually with increasing temperature, while the α-$Si_3N_4$ content decreases[29,32]. The Rietveld parameters ($\chi^2$, $R_{wp}$, $R_p$, and GoF) are presented in Table 1, demonstrating a coherent refinement of the X-ray diffraction data.

Figure 8 shows the compressive strength of the porous ceramics, with values of 59.36, 67.11, 72.57, and 73.14 MPa for samples sintered at 1550, 1600, 1650 , and 1700 °C, respectively. In addition, it is important to clarify that the theoretical strengths of α- and β-$Si_3N_4$ range from 51 to 63 GPa[33]. However, it is well known that the actual strength of ceramics is significantly lower than these theoretical values due to the presence of defects and microstructural imperfections. Even for fully dense silicon nitride ceramics, a compressive strength of around 4500 MPa is considered exceptionally high. This value is only achieved through advanced processing methods such as hot pressing (HPSN) and hot isostatic pressing (HIPSN), which can promote the development of a ceramic with 3.05-3.37 g/cm$^3$ of apparent density, besides a microstructure with complete α/β-$Si_3N_4$ transformation and minimal amounts of sintering aids[34]. For silicon nitride ceramics, beyond the impact of high porosity on mechanical performance, the presence of secondary phases also contributes to the compressive strength of the final ceramic composite. In the studied porous ceramics, the trace amount of $Ca_3SiO_5$ has a negligible effect on compressive strength. Wollastonite, on the other hand, may have a greater influence than $Ca_3SiO_5$, as the intensity of its peaks in the X-ray patterns indicates it is present in a higher concentration. A compressive strength of approximately 40 MPa for wollastonite was reported by AboAlmaged et al.[35].

The results show the potential of the studied porous ceramics for applications such as hot gas filters, catalyst supports, scaffolds for tissue engineering, and radio-transmitting devices, where compressive strength requirements are below 65 MPa[36-39]. Furthermore, as expected, this work demonstrates a gradual increase in the strength of the porous $Si_3N_4$ with rising sintering temperature due to the associated decrease in porosity. The equivalent pore size distribution curves shift to the left, indicating a reduction in average pore size resulting from the densification process. The porosity intentionally introduced within the ceramic structure acts as defects, weakening the

**Table 1.** Rietveld refinement statistics from the quantitative phase analysis of porous silicon nitride ceramics sintered at various temperatures, performed using PROFEX[21].

| | Sintering temperature (°C) | | | |
|---|---|---|---|---|
| | 1550 | 1600 | 1650 | 1700 |
| $R_{WP}$ | 14.96 | 12.39 | 14.49 | 10.33 |
| $R_{EXP}$ | 7.03 | 6.81 | 6.97 | 6.71 |
| $\chi^2$ | 4.53 | 3.31 | 4.32 | 2.37 |
| GoF | 2.13 | 1.82 | 2.08 | 1.54 |

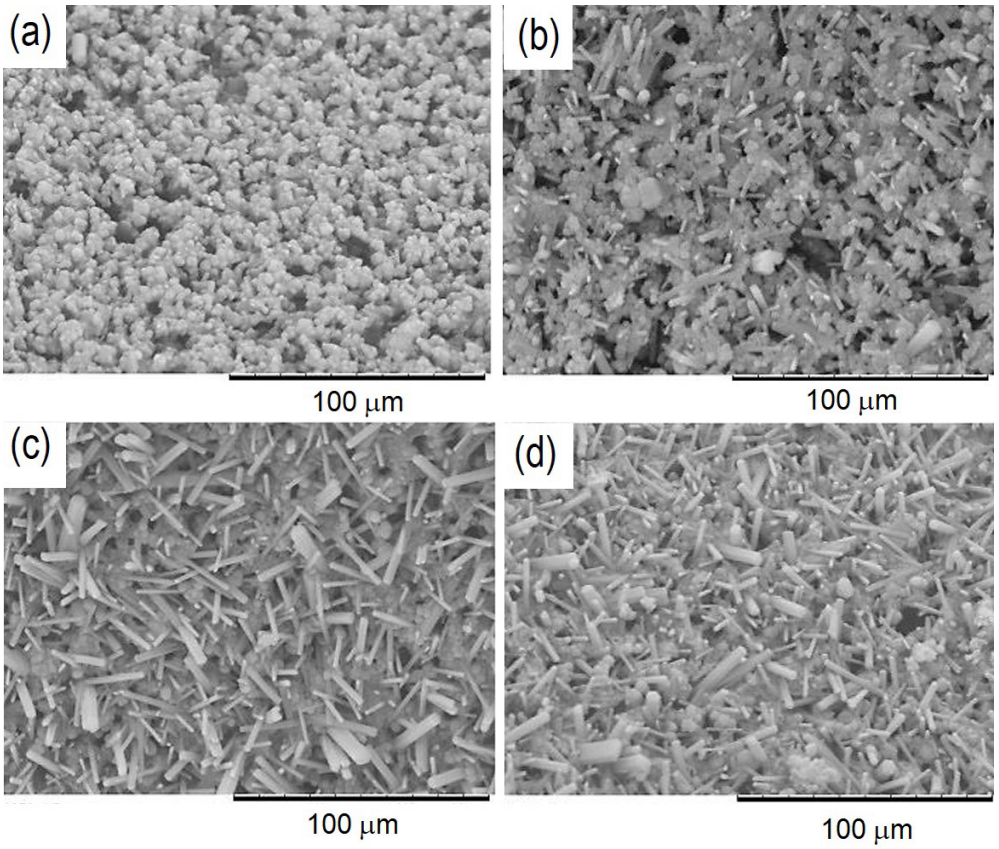


**Figure 5.** SEM images of the cell walls present in the silicon nitride ceramics sintered at a) 1550 °C, b) 1600 °C, c) 1650 °C and d) 1700 °C.

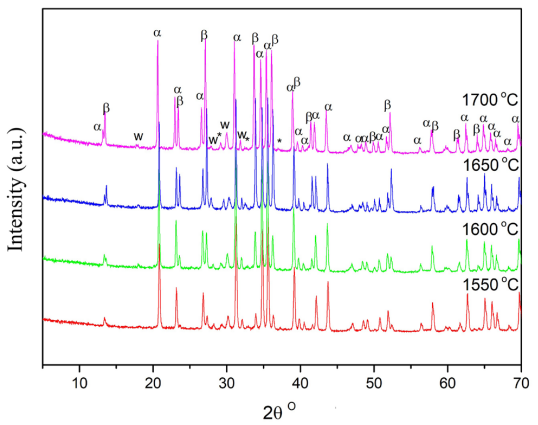


**Figure 6.** XRD spectra of the samples prepared at different sintering temperatures. α is α-$Si_3N_4$, β is β-$Si_3N_4$, w is $CaSiO_3$ and * is $Ca_3SiO_5$.

material by creating stress concentration regions[1]. On the other hand, increasing the sintering temperature from 1650 °C (72.57 MPa) to 1700 °C (73.14 MPa) did not result in an improvement in compressive strength. This behavior can be attributed to the ratio of β- to (α+β)-$Si_3N_4$ since these ratios are similar for the ceramics sintered at both temperatures.

In silicon nitride ceramics, the ratio of β- to (α+β)-$Si_3N_4$ has a significant impact on their compressive strength. Due to the three-dimensional network formed by the overlapping and interlocking β-$Si_3N_4$ columnar crystals, the presence of greater amounts of this phase in the microstructure typically results in increased strength[40].

It should be emphasized that we reached a good balance between porosity and strength. This can be confirmed by comparing the results of porosity (Figure 4) and compressive strength (Figure 8) with those of porous $Si_3N_4$ ceramics produced by other authors using the gelcasting technique. For example, we can cite Han et al.[41], who obtained $Si_3N_4$ foam ceramics with 68.9% of porosity, a pore size of 20–250 μm, and a compressive strength of 20.8 MPa, but using silicon as raw material and the microwave-nitridation method at 1273–1373. On the other hand, Moraes et al.[12] produced porous ceramics using $Si_3N_4$, $Y_2O_3$, and MgO as starting materials and agar as a gelling agent during the gelcasting step, followed by conventional sintering at 1600 °C. The samples presented an average cell size of 456 μm and cell window size of 79.18 μm and reached 86.1% of porosity but at the cost of a loss of compressive strength of 5 MPa. Using $Si_3N_4$, $Y_2O_3$, and $Al_2O_3$ as raw materials and white egg as a gelling agent, Li et al.[11] produced silicon nitride ceramics with a hierarchical structure with a pore size distribution of < 2 μm, 5-50 μm, and > 100 μm, high porosity of 76.3%, and

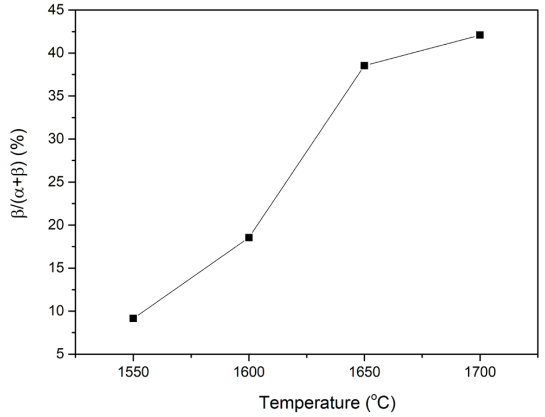


**Figure 7.** β/(α+β)-$Si_3N_4$ as function of the sintering temperature.

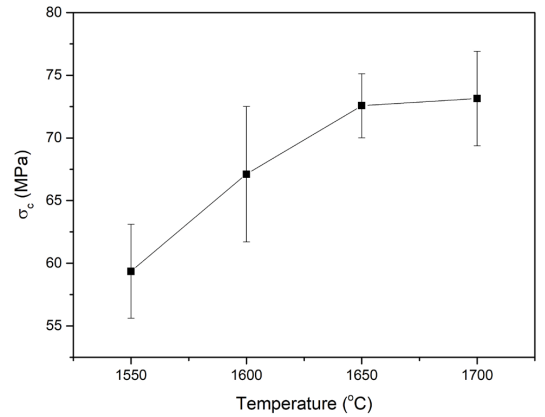


**Figure 8.** Compressive strength ($\sigma_c$) of the porous $Si_3N_4$ ceramics with respect of the sintering temperature.

18 MPa of compressive strength employing a low sintering temperature of 1550 °C. In our work, even the samples sintered at the lowest temperature of 1550 °C exhibited a compressive strength of ~59.36 MPa. This achievement may be attributed to the gelling agent (Isobam 110) adsorbed to the particle's surfaces through functional groups, forming bridges between various particles[42]. Additionally, the used additives formulation contributed to the favorable outcome, as they promoted a partial α/β-$Si_3N_4$ phase transformation, which became more pronounced at higher sintering temperatures.

## 4. Conclusion

Porous silicon nitride ceramics were effectively fabricated by combining gelcasting with pressureless sintering, using $SiO_2$ and CaO as sintering aids, with sintering temperatures ranging from 1550 to 1700°C for 1 hour. As the temperature increased, the proportion of β-$Si_3N_4$ to (α+β)-$Si_3N_4$ also increased. The bulk density of the porous samples ranged from 1 to 1.43 g/cm$^3$, while their apparent porosity ranged from 53.60 to 67.21%. The average pore size ranged from 89.20 to 158 µm. The compressive strength of the porous samples ranged from 59.36 to 73.14 MPa, decreasing as their porosity levels increased. Despite a porosity level of 67.21%, the compressive strength was still maintained at 59.36 MPa, which is in accordance with application as hot gas filters, catalyst supports, biomaterials, and radio-transmitting devices.

## 5. Acknowledgments

The authors acknowledge CNPq (Grant 144821/2024-9), CAPES (Grant 88887.857030/2023) and COPDE-IPEN (2020.06.IPEN.30) for their financial support.

## 6. References

1. Chen Y, Wang N, Ola O, Xia Y, Zhu Y. Porous ceramics: light in weight but heavy in energy and environment technologies. Mater Sci Eng Rep. 2021;143:100589. http://doi.org/10.1016/j.mser.2020.100589.
2. Hammel EC, Ighodaro OL-R, Okoli OI. Processing and properties of advanced porous ceramics: an application-based review. Ceram Int. 2014;40(10):15351-70. http://doi.org/10.1016/j.ceramint.2014.06.095.
3. Li X, Yu X, Yao D, Zuo K, Xia Y, Yin J, et al. Gas permeation performance of porous silicon nitride ceramics with controllable pore structures. Ceram Int. 2019;45(17):22351-6. http://doi.org/10.1016/j.ceramint.2019.07.264.
4. Cecen B, Topates G, Kara A, Akbulut SO, Havitcioglu H, Kozaci LD. Biocompatibility of silicon nitride produced via partial sintering & tape casting. Ceram Int. 2021;47(3):3938-45. http://doi.org/10.1016/j.ceramint.2020.09.257.
5. Du Z, Yao D, Xia Y, Zuo K, Yin J, Liang H, et al. The high porosity silicon nitride foams prepared by the direct foaming method. Ceram Int. 2019;45(2):2124-30. http://doi.org/10.1016/j.ceramint.2018.10.118.
6. Sun M, Yang S, Gao X, Man P, Qu J, Zhang W, et al. Structure and performance control of porous $Si_3N_4$ ceramics fabricated by freeze-drying process. Ceram Int. 2021;47(6):8169-74. http://doi.org/10.1016/j.ceramint.2020.11.174.
7. Parsi A, Golestani-Fard F, Mirkazemi SM. The effect of gelcasting parameters on microstructural optimization of porous $Si_3N_4$ ceramics. Ceram Int. 2019;45(8):9719-25. http://doi.org/10.1016/j.ceramint.2019.01.222.
8. Montanaro L, Coppola B, Palmero P, Tulliani J-M. A review on aqueous gelcasting: a versatile and low-toxic technique to shape ceramics. Ceram Int. 2019;45(7):9653-73. http://doi.org/10.1016/j.ceramint.2018.12.079.
9. Zou C, Guo S, Zhou X, Li S, Yan C, Shen T. Gel-casting prepared porous $Si_3N_4$ ceramics with different contents of $Y_2O_3$ and $Al_2O_3$ additives. J Mater Eng Perform. 2020;29(12):7891-8. http://doi.org/10.1007/s11665-020-05314-7.
10. Chen S, Wang L, He G, Li J, Wang CA. Microstructure and properties of porous $Si_3N_4$ ceramics by gelcasting–self-propagating high-temperature synthesis (SHS). J Adv Ceram. 2022;11(1):172-83. http://doi.org/10.1007/s40145-021-0525-7.
11. Li J, Yu Q, Li D, Zeng L, Gao S. Formation of hierarchical $Si_3N_4$ foams by protein-based gelcasting and chemical vapor infiltration. J Adv Ceram. 2021;10(1):187-93. http://doi.org/10.1007/s40145-020-0431-4.
12. Moraes EG, Innocentini MDM, Biasetto L, Oliveira APN, Hotza D, Colombo P. Gel casting of silicon nitride foams using biopolymers as gelling agents. Open Ceram. 2021;8:100183. http://doi.org/10.1016/j.oceram.2021.100183.
13. Yang Y, Shimai S, Wang S. Room-temperature gelcasting of alumina with a water-soluble copolymer. J Mater Res. 2013;28(11):1512-6. http://doi.org/10.1557/jmr.2013.132.

14. Wu Q, Li Y, Zhang B, Liu Y, Li X, Ji H. A new gelcasting using Isobam both as dispersant and monomer. Ceram Int. 2023;49(10):15560-7. http://doi.org/10.1016/j.ceramint.2023.01.145.
15. Wan T, Yao D, Hu H, Xia Y, Zuo K, Zeng Y. Fabrication of porous $Si_3N_4$ ceramics through a novel gelcasting method. Mater Lett. 2014;133:190-2. http://doi.org/10.1016/j.matlet.2014.06.182.
16. Wan T, Yao D, Yin J, Xia Y, Zuo K, Zeng Y. The microstructure and mechanical properties of porous silicon nitride ceramics prepared via novel aqueous gelcasting. Int J Appl Ceram Technol. 2015;12(5):932-8. http://doi.org/10.1111/ijac.12424.
17. Wan T, Yao D, Yin J, Xia Y, Zuo K, Liang H, et al. Novel method for preparing $Si_3N_4$ ceramics with unidirectional oriented pores from silicon aqueous slurries. J Eur Ceram Soc. 2017;37(10):3285-91. http://doi.org/10.1016/j.jeurceramsoc.2017.04.013.
18. Steel Institute VDEh. Slag Atlas. 2nd ed. Düsseldorf: Verlag Stahleisen GmbH; 1995.
19. Guedes-Silva CC, Rodas ACD, Silva AC, Ribeiro C, Carvalho FMS, Higa OZ, et al. Microstructure, mechanical properties and *in vitro* biological behavior of silicon nitride ceramics. Mater Res. 2018;21(6):e20180266. http://doi.org/10.1590/1980-5373-mr-2018-0266.
20. Schneider C, Rasband W, Eliceiri K. NIH Image to ImageJ: 25 years of image analysis. Nat Methods. 2012;9(7):671-5. http://doi.org/10.1038/nmeth.2089.
21. Doebelin N, Kleeberg R. Profex: a graphical user interface for the Rietveld refinement program BGMN. J Appl Cryst. 2015;48(5):1573-80. http://doi.org/10.1107/S1600576715014685.
22. Torki M, Movahedi B, Ghazanfari S, Milani M. Fabrication and mechanical characterization of YAG ceramic composite with alumina nanoparticles using slip casting and sintering process. Mater Res Express. 2020;7(11):115010. http://doi.org/10.1088/2053-1591/abca6b.
23. Zhang X, He J, Han L, Huang Z, Xu K, Cai W, et al. Foam gel-casting preparation of SiC bonded $ZrB_2$ porous ceramics for high-performance thermal insulation. J Eur Ceram Soc. 2023;43(1):37-46. http://doi.org/10.1016/j.jeurceramsoc.2022.09.055.
24. Tang SJ, Zeng XM, Huang KH, Guo WM, Yu JJ, Lin HT. Effect of $ZrB_2$ on promoting the phase transformation mechanism of $Si_3N_4$-based ceramics at low temperature. Ceram Int. 2023;49(19):31439-44. http://doi.org/10.1016/j.ceramint.2023.07.091.
25. He L, Huang N, Lu D, Sheng P, Zou W. A study on the effects of liquid phase formation temperature and the content of sintering aids on the sintering of silicon nitride ceramics. Crystals. 2023;13(7):1099. http://doi.org/10.3390/cryst13071099.
26. Caslavsky JL, Viechnicki DJ. Melting behaviour and metastability of yttrium aluminium garnet (YAG) and $YAlO_3$ determined by optical differential thermal analysis. J Mater Sci. 1980;15(7):1709-18. http://doi.org/10.1007/BF00550589.
27. Kingery WD. Densification during sintering in the presence of a liquid phase. I. Theory. J Appl Phys. 1959;30(3):301-6. http://doi.org/10.1063/1.1735155.
28. Hampshire S. Silicon nitride ceramics. Mater Sci Forum. 2008;606:27-41. http://doi.org/10.4028/www.scientific.net/MSF.606.27.
29. Yin S, Zhang Y, Wan W, Fang X, Ma H, Xie X, et al. Effects of sintering temperature and sintering additive on microstructure, mechanical and dielectric properties of porous $Si_3N_4$ ceramics by gelcasting. J Alloys Compd. 2024;979:173560. http://doi.org/10.1016/j.jallcom.2024.173560.
30. Kota N, Roy S. Effect of $H_3PO_4$ content and processing temperature on the structure and mechanical properties of porous $Si_3N_4$. Ceram Int. 2023;49(23):37174-86. http://doi.org/10.1016/j.ceramint.2023.09.041.
31. Kramer M, Wittmüss D, Küppers H, Hoffman MJ, Petzow G. Relations between crystal structure and growth morphology of beta-$Si_3N_4$. J Cryst Growth. 1994;140(1-2):157-66. http://doi.org/10.1016/0022-0248(94)90509-6.
32. Wang L, Wang L, Hao Z, Tang W, Dou R. Microstructure and properties of silicon nitride ceramics fabricated by vat photopolymerization in combination with pressureless sintering. Ceram Int. 2024;50(7):10485-96. http://doi.org/10.1016/j.ceramint.2023.12.361.
33. Csanádi T, Gall M, Vojtko M, Kovalčíková A, Hnatko M, Dusza J, et al. Micro scale fracture strength of grains and grain boundaries in polycrystalline La-doped β-$Si_3N_4$ ceramics. J Eur Ceram Soc. 2020;40(14):4783-91. http://doi.org/10.1016/j.jeurceramsoc.2020.04.033.
34. Krstic Z, Krstic VD. Silicon nitride: the engineering material of the future. J Mater Sci. 2012;47(2):535-52. http://doi.org/10.1007/s10853-011-5942-5.
35. Abo-Almaged HH, Ngida REA, Ajiba NA, Sadek HEH, Khattab RM. Utilization of industrial waste materials for the preparation of wollastonite by temperature induced forming technique. Sci Rep. 2024;14(1):21752. http://doi.org/10.1038/s41598-024-71243-3.
36. Gregorovičová E, Pospísil J. Ceramic filters for high-temperature flue gas filtration and their regeneration: a review of the current state of knowledge. Process Saf Environ Prot. 2024;190:688-703. http://doi.org/10.1016/j.psep.2024.07.088.
37. Mahmoudian M, Hemmati A, Hashemabadi H, Ghaemi A, Shahhosseini S. Investigation of salt and precipitating agent effect on the specific surface area and compressive strength of alumina catalyst support. Pol J Chem Technol. 2017;19(3):35-40. http://doi.org/10.1515/pjct-2017-0045.
38. Rajakaruna RADNV, Asmatulu E. Recent progress in low-dielectric constant materials in the aviation industry: a review. IEEE Trans Dielectr Electr Insul. 2024;31(5):2365-72. http://doi.org/10.1109/TDEI.2024.3377177.
39. Chen Q, Baino F, Spriano S, Pugno N, Vitale-Brovarone C. Modelling of the strength-porosity relationship in glass-ceramic foam scaffolds for bone. J Eur Ceram Soc. 2014;34(11):2663-73. http://doi.org/10.1016/j.jeurceramsoc.2013.11.041.
40. Yang F, Yao Y, Yang Z, Zhao S, Chen G, Li K. Fabrication of in-situ self-reinforced $Si_3N_4$ ceramic foams for high-temperature thermal insulation by protein foaming method. Ceram Int. 2021;47(13):18351-7. http://doi.org/10.1016/j.ceramint.2021.03.156.
41. Han L, Li F, Huang L, Zhang H, Pei Y, Dong L, et al. Preparation of $Si_3N_4$ porous ceramics via foam-gelcasting and microwave nitridation method. Ceram Int. 2018;44(15):17675-80. http://doi.org/10.1016/j.ceramint.2018.06.231.
42. Mao D, Yin S, Fang X, Wang Y, Li Q, Yang J. Preparation and properties of fused silica ceramics by Isobam spontaneous coagulation casting. Ceram Int. 2022;48(4):5130-8. http://doi.org/10.1016/j.ceramint.2021.11.051.


## Data Availability

All data are provided within the manuscript.